ACS APPLIED MATERIALS & INTERFACES

www.acsami.org

Research Article

N-Type Doping of Naphthalenediimide-Based Random Donor−Acceptor Copolymers to Enhance Transistor Performance and Structural Crystallinity

Yun Chang,[⊥] Ying-Sheng Wu,[⊥] Shih-Huang Tung, Wen-Chang Chen, Chu-Chen Chueh,* and Cheng-Liang Liu*

Cite This: *ACS Appl. Mater. Interfaces* 2023, 15, 15745−15757

Read Online

ACCESS | Metrics & More | Article Recommendations | Supporting Information

ABSTRACT: An integrated strategy of molecular design and conjugated polymer doping is proposed to improve the electronic characteristics for organic field effect transistor (OFET) applications. Here, a series of soluble naphthalene diimide (**NDI**)-based random donor−acceptor copolymers with selenophene π-conjugated linkers and four acceptors with different electron-withdrawing strengths (named as **rNDI-N/S/NN/SS**) are synthesized, characterized, and used for OFETs. N-type doping of **NDI**-based random copolymers using (12*a*,18*a*)-5,6,12,12*a*,13,18,18*a*,19-octahydro-5,6-dimethyl-13,18[1′,2′]-benzenobisbenzimidazo[1,2-*b*:2′,1′-*d*]benzo[*i*][2.5]benzodiazocine potassium triflate adduct (**DMBI-BDZC**) is successfully demonstrated. The undoped **rNDI-N**, **rNDI-NN**, and **rNDI-SS** samples exhibit ambipolar charge transport, while **rNDI-S** presents only a unipolar n-type characteristic. Doping with **DMBI-BDZC** significantly modulates the performance of **rNDI-N/S** OFETs, with a 3- to 6-fold increase in electron mobility (μ_e) for 1 wt % doped device due to simultaneous trap mitigation, lower contact resistance (R_C), and activation energy (E_A), and enhanced crystallinity and edge-on orientation for charge transport. However, the doping of intrinsic pro-quinoidal **rNDI-NN/SS** films exhibits unchanged or even reduced device performance. These findings allow us to manipulate the energy levels by developing conjugated copolymers based on various acceptors and quinoids and to optimize the dopant−polymer semiconductor interactions and their impacts on the film morphology and molecular orientation for enhanced charge transport.

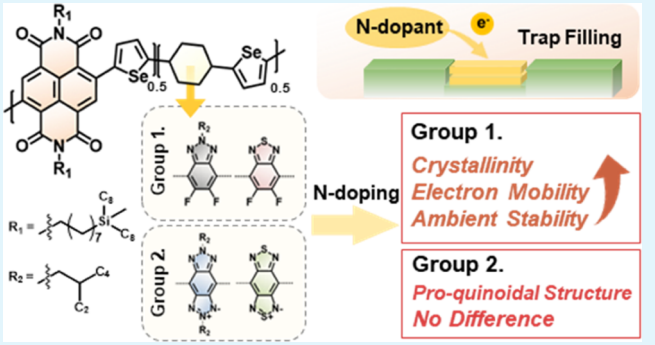

KEYWORDS: *naphthalene diimide, doping, donor−acceptor, ambipolar, organic field effect transistors*

INTRODUCTION

In recent decades, organic optoelectronic devices, such as memristors,[1−4] light-emitting diodes (LEDs),[5,6] solar cells,[7−9] and field effect transistors (FETs),[10−18] have achieved rapid progress. Behind this, the intense development of conjugated polymers has played the most critical role. It is well known that conjugated polymers possess the advantages of high structural diversity, light weight, and facile solution processability, which opens a bright future for the development of soft electronics. Among the structural designs of conjugated polymers that have been exploited, donor−acceptor (D−A) design has become the most common strategy to achieve small band gap values and good charge transport properties as a result of the intramolecular charge transfer effects of electron-rich (as donor molecules) and electron-deficient monomers (as acceptor molecules).[17,19−22] Furthermore, the backbone and/or side-chain structures can be fine-tuned to precisely manipulate the optoelectronic characteristics of the derived polymers. Due to these attractive features, numerous D−A-type conjugated polymers have been designed and reported in the literature.[23,24]

It should be noted that the development of D−A-type conjugated polymers is dictated by the development of both donor and acceptor cores. Compared to the diverse designs of donor cores, the designs of acceptor cores are relatively monotonous. Only a few acceptor cores are widely used, and the naphthalene diimide (**NDI**) unit is one of the most symbolic and promising n-type cores.[25−30] A number of **NDI**-derived polymers have been developed to achieve high-performance organic field effect transistors (OFETs).[31−33] One reason is that the inclusion of imide group gives **NDI**-

Received: December 25, 2022
Accepted: March 8, 2023
Published: March 15, 2023

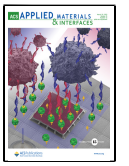

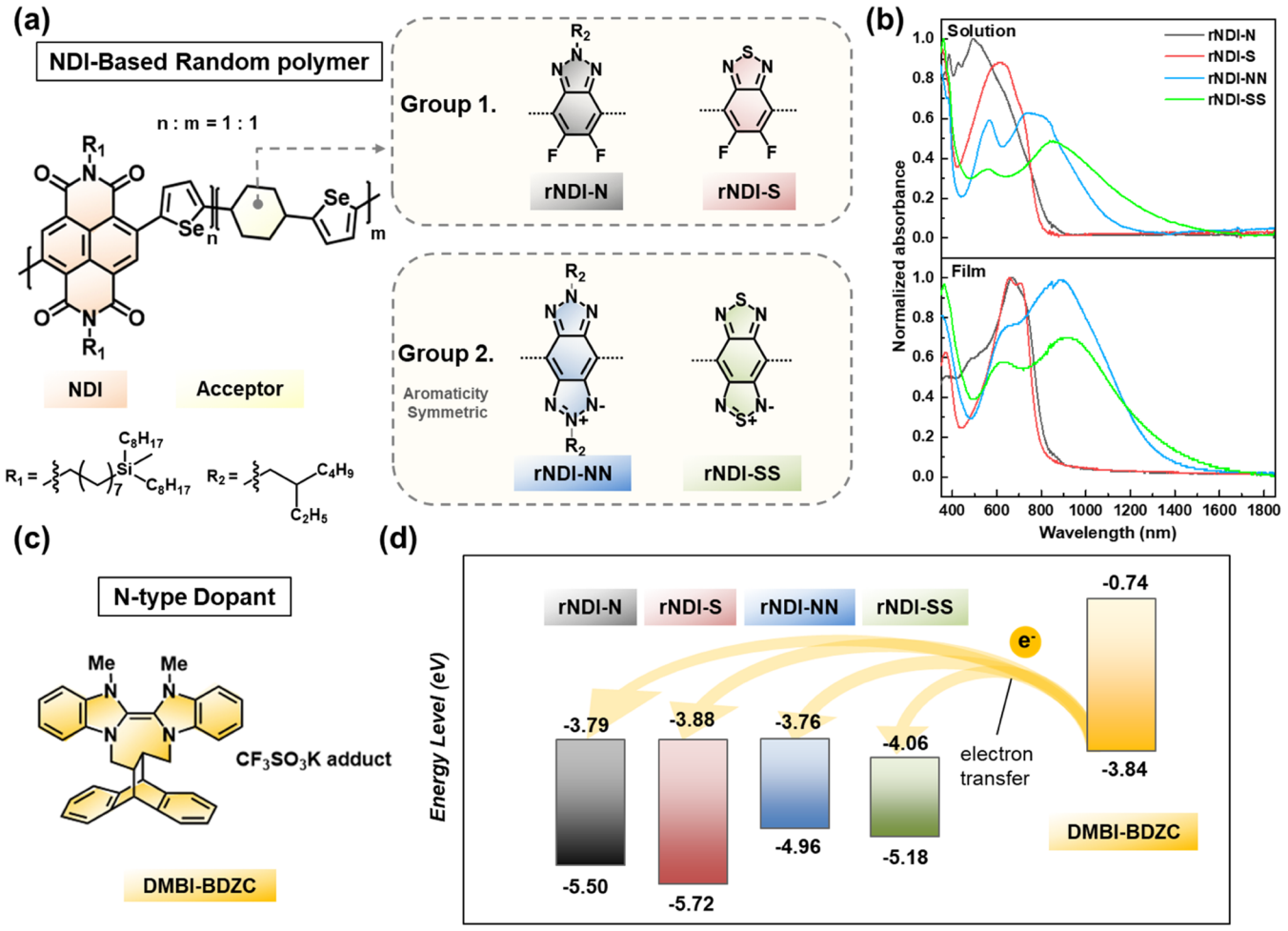

Figure 1. (a) Molecular structures of **rNDI**-based polymers. (b) UV−vis−IR spectra of rNDI-based polymers. (c) Molecular structures of **DMBI-BDZC**. (d) Energy level of rNDI-based polymers and **DMBI-BDZC** dopant.

based backbones a relatively deep energy level and strong electron-withdrawing ability, which leads to an extremely electron-deficient property. The outstanding coplanarity due to the advanced aromaticity of the **NDI** core is another key factor in achieving high charge transport properties.

Note that although the progress of acceptor cores has been slower than that of donor cores, a principle for designing efficient n-type conjugated polymers has recently switched from the typical D−A design to an A−A design; that means the copolymerization of two different acceptor cores. It has been shown that the combination of two electron-deficient molecules provides stronger intramolecular interactions to improve charge transport properties. For instance, Wang et al. have prepared a series of dual-acceptor conjugated polymers by coupling the **NDI** unit to strong acceptor units such as benzothiadiazole and triazolobenzothiadiazole via vinylene bridges. Through the strong interlock effect created by the hydrogen bonding between the vinylene bridge and the imide group on the **NDI** moiety or the fluorine atom on the acceptors, the remarkable coplanarity of the conjugated backbone of target polymers can be controlled, thus greatly improving the transistor performance. Their novel dual-acceptor design based on **NDI** and strong acceptors demonstrated an impressive electron mobility of 7.37 $cm^2 V^{-1} s^{-1}$.[31] Inspired by these results, we are interested in developing a series of **NDI**-based dual-acceptor conjugated polymers for OFETs.

Recent studies have shown that benzothiadiazole, benzotriazole, benzobisthiadiazole, and benzobistriazole are promising acceptor cores for achieving high-performance OFETs.[34−36] In particular, the pro-quinoidal feature of benzobisthiadiazole and benzobistriazole have been shown to enhance charge mobility and doping. Given this unique advantage, it will be interesting to couple **NDI** units with these emerging acceptor units to develop a new series of n-type conjugated polymers. On the other hand, rather than constructing conventional alternating conjugated copolymers, we intend to prepare random copolymers based on these acceptor cores. The main reason for this is the solubility issue. Random copolymers have been demonstrated to have low long-range crystallinity, which facilitates the solubility of the derived polymers. However, for some random copolymers, the reduction in long-range crystallinity does not disrupt the degree of aggregation of the short-range chains and maintains high OFET performance.[37,38] In addition, the reduction in long-range crystallinity also promotes dopant tolerance of the derived polymers to improve electrical conductivity.

In the case of OFETs, the solution doping process is also thought to lead to improvements in device parameters, including reduced contact resistance, improved bias stability, and increased charge carrier mobility.[39−44] One limitation is

https://doi.org/10.1021/acsami.2c23067
ACS Appl. Mater. Interfaces 2023, 15, 15745−15757

that while p-type doping of organic semiconductors has been extensively studied, n-type doping is rather limited. This is because doping via the conventional ground-state integer charge transfer (ICT) process requires the donation of electrons from the highest occupied molecular orbital (HOMO) of the dopant to the lowest unoccupied low orbital (LUMO) of the host semiconductor.[45] This synthesis is challenging because the dopant needs to have a high HOMO value and be stable in air. To overcome these challenges, recently, Anthopoulos and co-workers used an n-type dopant (Figure 1c), namely, [1,2-*b*:2′,1′-*d*]benzo[*i*][2.5]-benzodiazocine potassium triflate adduct (**DMBI-BDZC**), based on its electron-rich ethylenediamine core, as this electron-rich alkene is a known n-type dopant, and also based on its low vapor pressure crystalline solid and matching HOMO energy level. Its HOMO and LUMO levels are shown in Figure 1d.[46] The potential of **rNDI**-based polymers was investigated by developing postdoping conjugated copolymers based on various acceptors and quinones. Microstructural analysis of organic semiconductor channels by atomic force microscopy (AFM) and grazing incidence wide-angle X-ray scattering (GIWAXS) measurements showed a significant impact on the molecular orientation and crystallinity in **rNDI**-based polymers. OFET measurements performed as a function of temperature provide further evidence of n-type doping, showing a decrease in contact resistance (R_C) and activation energy (E_A) and an increase in electron mobility (μ_e) under n-type doping.

EXPERIMENTAL SECTION

Materials and Synthesis. All of the commercially available reagents were purchased from Sigma-Aldrich unless otherwise stated. 4,7-Dibromo-5,6-difluoro-2,1,3-benzothiadiazole (**S**), 4,7-dibromo-2-(2-ethylhexyl)-5,6-difluoro-2*H*-benzotriazole (**N**), and 4,8-dibromo-benzo[1,2-*c*:4,5-*c*′]bis([1,2,5]thiadiazole) (**SS**) monomers were purchased from Luminescence Technology Corp. **DMBI-BDZC** n-type dopant was purchased from Strem Chemicals. The detailed synthetic procedures for monomers (2,5-bis(trimethylstannyl)selenophene (**M1**), methyl(8-bromooctyl)-dioctylsilane (**NDI-SiC8**), and 4,8-dibromo-2,6-bis(2-ethylhexyl)-benzo[1,2-*d*:4,5-*d*′]bis([1,2,3]triazole) (**NN**)) are presented in the Supporting Information, according to the methods reported in the literature.[30]

Polymerization of the Targeted Random Copolymers. The monomers **M1** as well as **NDI-SiC8** and **S**/**N**/**SS**/**NN** (both 0.5 equiv with respect to **M1**) were dissolved in chlorobenzene (0.1 M) with the addition of $Pd(PPh_3)_4$ (5 mol % with respect to **M1**) and sealed in a microwave vessel in a nitrogen-filled glovebox. The polymerization was conducted at 160 °C for 90 min through Stille coupling under microwave heating. The end-capping reaction proceeded at 160 °C for 15 min afterward by adding 2-(tributylstannyl)thiophene and 2-bromothiophene consecutively (both 1.1 equiv with respect to **M1**). After cooling to room temperature, the reaction mixture was poured into methanol, followed by the collection of the resulting precipitate. Soxhlet extraction through acetone and hexane was then proceeded to remove the remaining catalyst and the oligomers. The final product was extracted by chloroform, and the concentrated solution was poured into methanol to precipitate polymers. After filtration and drying under vacuum, the polymers were finally obtained.

Synthesis of rNDI-S. Dark solid (yield: 44.8%). Anal. calcd for $[C_{78}H_{112}F_2N_4O_4SSe_2Si_2]$: C, 64.4; H, 7.9; N, 3.9; S, 2.2. Found: C, 62.2; H, 7.4; N, 4.1; S, 2.4. Molecular weight evaluated by GPC: M_n = 12.0 kDa, M_w = 34.0 kDa, $Đ$ = 2.90. ^{1}H NMR spectra are displayed in Figure S6.

Synthesis of rNDI-N. Dark solid (yield: 41.1%). Anal. calcd for $[C_{86}H_{129}F_2N_5O_4Se_2Si_2]$: C, 66.6; H, 8.5; N, 4.5. Found: C, 68.7; H, 8.9; N, 4.3. Molecular weight evaluated by GPC: M_n = 13.0 kDa, M_w = 34.0 kDa, $Đ$ = 2.58. ^{1}H NMR spectra are displayed in Figure S7.

Synthesis of rNDI-SS. Dark solid (yield: 38.4%). Anal. calcd for $[C_{78}H_{112}N_6O_4S_2Se_2Si_2]$: C, 63.4; H, 7.8; N, 5.7; S, 4.3. Found: C, 61.2; H, 7.2; N, 5.8; S, 4.2. Molecular weight evaluated by GPC: M_n = 8.8 kDa, M_w = 15.0 kDa, $Đ$ = 1.70. ^{1}H NMR spectra are displayed in Figure S8.

Synthesis of rNDI-NN. Dark solid (yield: 33.6%). Anal. calcd for $[C_{94}H_{146}F_2N_8O_4Se_2Si_2]$: C, 67.7; H, 8.9; N, 6.7. Found: C, 69.6; H, 9.3; N, 6.3. Molecular weight evaluated by GPC: M_n = 8.3 kDa, M_w = 16.0 kDa, $Đ$ = 1.91. ^{1}H NMR spectra are displayed in Figure S9.

OFET Fabrication and Measurement. Polymer semiconductor solutions were prepared by dissolving **rNDI**-based polymers in anhydrous chloroform (CF) solution at a concentration of 10 mg mL^{-1}, while **DMBI-BDZC** was prepared in CF, both in an inert nitrogen-filled glovebox. The **DMBI-BDZC** solution was added to the polymer solution at varying weight percentages from 0.5 to 4 wt % (1, 3, 3.5 wt % for **rNDI-N**, 1, 3, 4 wt % for **rNDI-S**, 0.5, 1 wt % for **rNDI-NN**, 1 wt % for **rNDI-SS**). The doped polymer solutions were heated at 55 °C overnight in the glovebox before solution deposition the next day. All Si/SiO_2 substrates were cleaned using acetone and isopropanol for 5 min in each by sonication in an ultrasonic bath, dried with a gentle stream of nitrogen, followed by treatment in a Harrick plasma cleaner PDC-32G set to a high RF level for 5 min. Then, the substrates were immersed in a prepared octadecyltrichlorosilane (ODTS; 4 μL mL^{-1} in anhydrous toluene) for 90 min to form the coverage of ODTS self-assembly monolayers (SAMs) on SiO_2 surfaces. Doped **rNDI**-based conjugated polymer films were solution-sheared at ambient conditions with a shearing speed of 3 mm s^{-1} and deposited temperature of 25 °C according to our previous report,[47] producing thicknesses of ∼50 nm (obtained from a KLA-Tencor alpha-step D-300 profilometer). Following that, the devices were annealed at 160 °C for 15 min in the glovebox before thermal evaporation of Au as source/drain contacts at 25 and 1500 nm channel length (L) and width (W), respectively.

All electrical measurements were carried out in a nitrogen-filled glovebox at room temperature and in the dark using a Keithley 4200-SCS semiconductor characterization system. The field effect mobility (μ) and threshold voltage (V_{th}) were extracted from the slope and intercept of the curves based on the square root of drain current (I_d) vs gate voltage (V_g), respectively, according to the following equation

$$(I_d)^{1/2} = \frac{W\mu C_i}{2L}(V_g - V_{th}) \quad (1)$$

where C_i is the capacitance per unit area of the SiO_2 dielectric layer.

RESULTS AND DISCUSSION

Synthesis and Characterization of the Studied Polymers. As displayed in Figure 1a, a series of **NDI**-based dual-acceptor random copolymers are designed and synthesized. We randomly copolymerized an **NDI-SiC8** moiety with four different second acceptor moieties, including benzothiadiazole (**S**), benzotriazole (**N**), benzo[1,2-*c*:4,5-*c*′]bis[1,2,5]-thiadiazole (**SS**), and benzo[1,2-*d*:4,5-*d*′]bis[1,2,3]triazole (**NN**), respectively. Notably, instead of using the conventional branched alkyl side chain, we herein attached the silane side chain to the **NDI** moiety (**NDI-SiC8**) to give the prepared polymers higher solubility and better chain packing ability.[48] The synthetic route for **NDI-SiC8** is depicted in Scheme S1, and the details are described in the Experimental Section. Also, we used a selenophene spacer (**M1**) instead of the conventional thiophene spacer in the random polymerization process. This is because the electron affinity of selenium is stronger than that of sulfur, which potentially favors the intrachain charge transfer on the backbone.[49] In addition, the larger size of selenium than sulfur facilitates soothing the space between the highly rigid acceptor moieties to promote chain packing.[50]

https://doi.org/10.1021/acsami.2c23067
ACS Appl. Mater. Interfaces 2023, 15, 15745−15757

Table 1. Thermal, Optical, and Electrochemical Properties of Undoped rNDI-Based Polymers

	M_n (kDa)[a]	M_w (kDa)[a]	$Đ$[a]	λ_{max} (nm)[b]	E_g (eV)[c]	HOMO (eV)[d]	LUMO (eV)[e]	$T_d^{5\%}$ (°C)[f]
rNDI-S	12.0	34.0	2.90	640	1.84	−5.72	−3.88	398
rNDI-N	13.0	34.0	2.58	658	1.71	−5.50	−3.79	400
rNDI-SS	8.8	1.50	1.70	360/625/924	1.12	−5.18	−4.06	365
rNDI-NN	8.3	1.60	1.91	628/845	1.26	−5.10	−3.84	373

[a]M_n, M_w, and $Đ$ values were measured by SEC eluted by dichlorobenzene. [b]Thin-film UV−vis absorption maxima. [c]The optical E_g values were evaluated from the absorption onset of polymer films deposited on quartz substrates. [d]CV was recorded using Fc/Fc^+ as an internal potential reference. [e]Estimated by LUMO = HOMO + E_g. [f]Determined from the thermogravimetric analysis (TGA) curve at 5% weight loss.

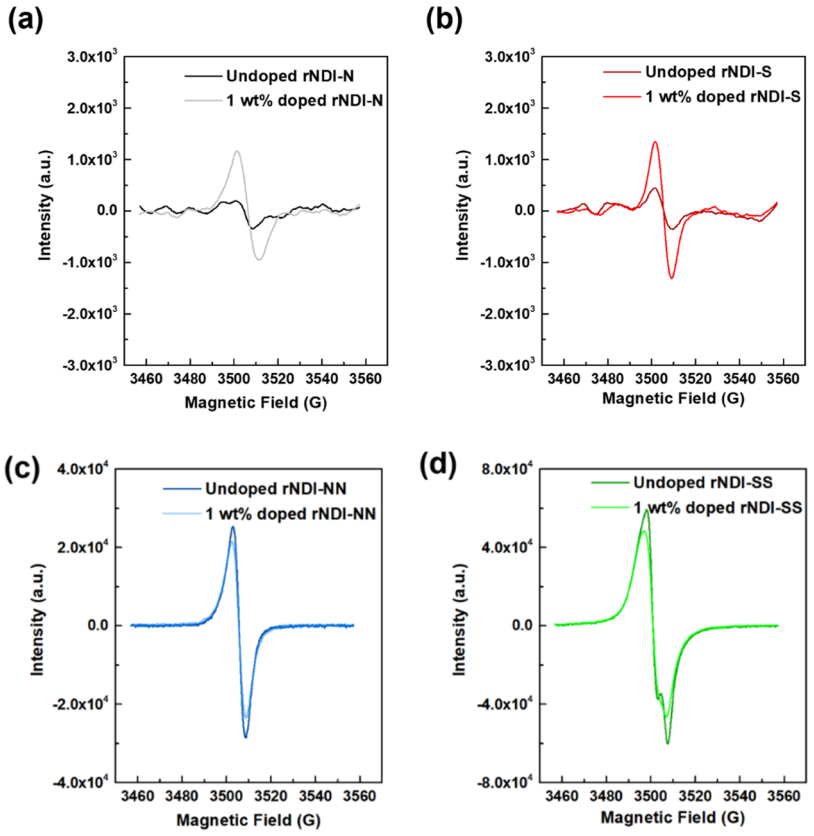

Figure 2. EPR spectra of the (a) **rNDI-N**, (b) **rNDI-S**, (c) **rNDI-NN**, and (d) **rNDI-SS** solution undoped and doped with 1 wt % dopant concentrations.

For the monomers employed, **M1**, **NN**, and **NDI-SiC8** were synthesized according to the methods reported in the literature, except for **S**, **N**, and **SS**.[36] The signals at 7.7 and 0.4 ppm in the ^{1}H NMR spectrum of **M1** (Figure S1) represent proton on the selenophene and proton next to tin attached to the selenophene moiety, respectively. In addition, the signals at 9.0 and 4.2 ppm in the ^{1}H NMR spectrum of **NDI-SiC8** (Figure S5) represent the proton on the naphthalene ring and the proton next to the nitrogen on the imide structure, respectively. Similarly, in the ^{1}H NMR spectrum of **NN** (Figure S2), the signal at 4.8 ppm represents the proton next to the nitrogen on the triazole structure on the **NN** unit. The signals calculated from the integration were highly correlated with the target structures, indicating the successful preparation of the monomers.

Four **NDI**-based dual-acceptor random copolymers, **rNDI-S/N/SS/NN**, were prepared via Stille coupling, coupling **NDI-SiC8** and **M1** to **S/N/SS/NN**, respectively, where the stoichiometric ratio for the two acceptor moieties is 0.5 equiv with respect to **M1**. Details of the polymerization are described in the Supporting Information. Figures S6−S9 show the ^{1}H NMR spectra of **rNDI-S/N/SS/NN**, clearly confirming the successful polymerization of the target polymers. The molecular weight values of these synthesized polymers were determined by GPC eluted with *o*-DCB, and the results are summarized in Table 1. All of these polymers have good solubility in common solvents due to the silane side chain on the **NDI** moiety and the random backbone design. These polymers also exhibit good thermal properties. As shown in Figure S11, no obvious thermally induced decomposition was observed until 360 °C. They were then examined by differential scanning calorimetry (DSC) for thermally induced phase transitions. As shown in Figure S12, no conspicuous phase change was evident between 0 and 250 °C. The high thermal decomposition temperature and negligible phase transition of these polymers are attributed to their high backbone rigidity and sufficient molecular weight.

Optical and Electrochemical Properties. Figure 1b shows the UV−vis−IR spectra of the studied polymers in solution and film states, while Figure 1d displays the relative

https://doi.org/10.1021/acsami.2c23067
ACS Appl. Mater. Interfaces 2023, 15, 15745−15757

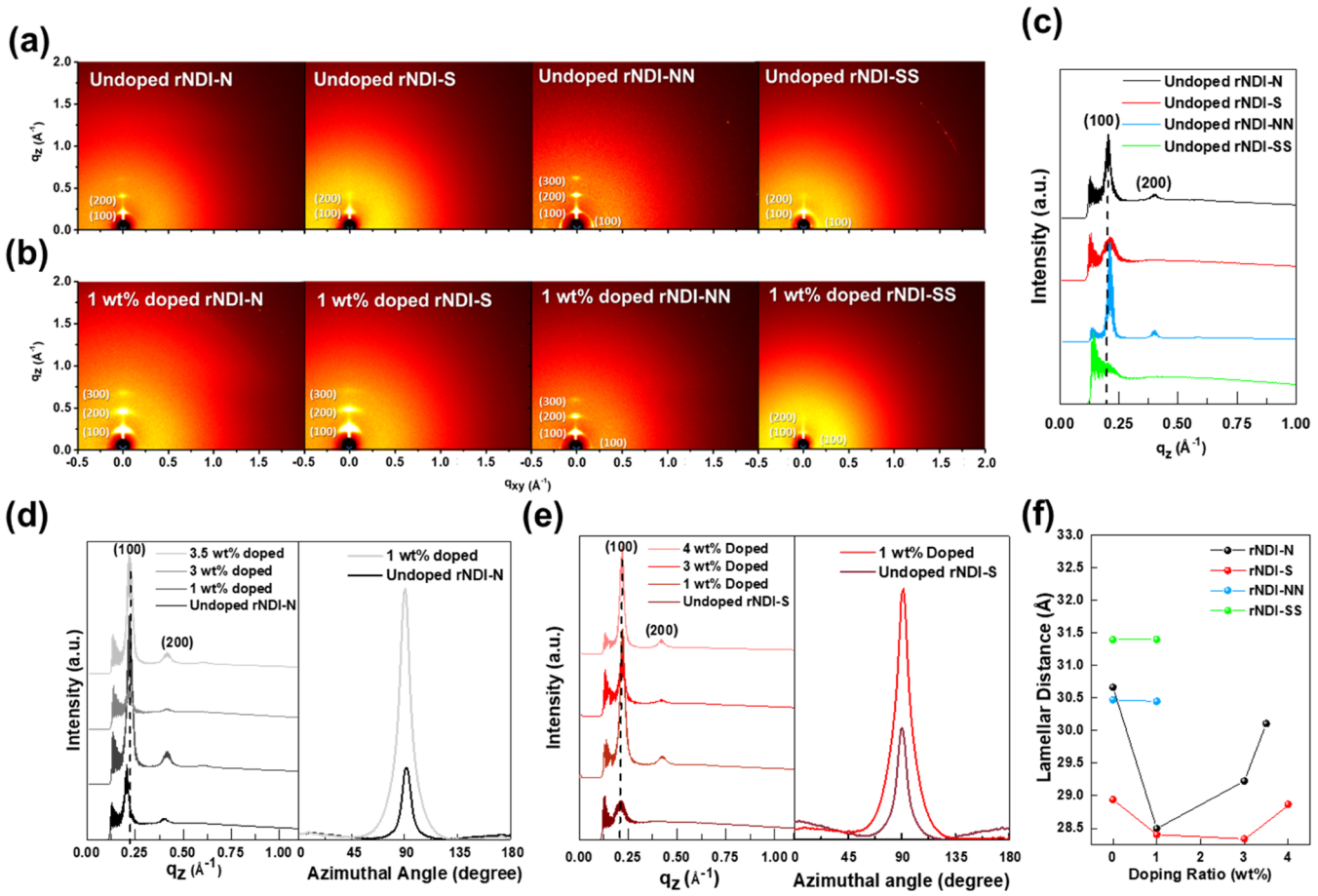

Figure 3. 2D GIWAXS of (a) undoped and (b) 1 wt % doped **rNDI**-based polymer. Out-of-plane diffraction profiles extracted along the q_z direction of (c) undoped four **rNDI**-based polymers, (d) **rNDI-N**, and (e) **rNDI-S** with dopant concentrations varying from 0 to 4 wt %. Azimuthal angle of (d) **rNDI-N** and (e) **rNDI-S** with dopant concentrations in 1 wt %. The lamellar structures with the characteristic diffraction peaks (100) in comparisons with (f) four **rNDI**-based polymer films undoped and doped with dopant concentrations varying from 0 to 4 wt %.

energy levels of the random D−A copolymers. By deriving the spectra, the band gaps of all four polymers are calculated and summarized in Table 1. In the film spectra, a clear 0-0 stacking peak is observed in the **rNDI-S** film, indicating that only **rNDI-S** possesses a significant aggregation behavior. Regarding the differences between solution and film spectra, the triazole-based polymers (**N** and **NN**) show obvious differences, which is related to their different backbone packing behavior because of the additional side chains in the triazole moiety. The above phenomenon of backbone packing patterns will be further described in the morphology section. The thiadiazole and triazole groups also produced differences in the two spectra. **rNDI-SS** shows a red-shifted spectrum compared to **rNDI-NN**, which is attributed to a stronger electron-withdrawing ability. However, no significant difference was observed between **rNDI-N** and **rNDI-S**. Since the presence of fluorine atoms imparts a strong electron-withdrawing ability to both acceptor moieties, the effect of replacing the thiadiazole with a triazole is mitigated. The electron-withdrawing ability also influenced the difference in HOMO/LUMO levels. The highest occupied molecular orbit (HOMO) energy level for each material was derived from cyclic voltammetry (CV) (Figure S13), where HOMO = 4.8 − ΔE. ΔE was calculated by measuring the difference between the onset of oxidation and the half-wave potential of the ferrocene standard. The lowest unoccupied molecular orbit (LUMO) energy level was derived from the difference between the HOMO level and the optical band gap, i.e., LUMO = HOMO − optical band gap. The LUMO level is determined by the LUMO level of its stronger acceptor moiety; thus, polymers containing thiadiazoles show lower HOMO/LUMO levels than triazole-based polymers. The HOMO/LUMO levels for **rNDI-S/N/SS/NN** were found to be −5.50/−3.79, −5.72/−3.88, −4.96/−3.76, and −5.18/−4.06 eV, respectively. However, for the reasons mentioned above, the decrease from **N** to **S** is smaller compared to the difference between **NN** and **SS**. **rNDI-S/N/SS/NN** have band gaps of 1.84, 1.71, 1.12, and 1.26 eV respectively. The band gap of the polymer decreases to a large extent as the aromaticity of the acceptor moiety increases. With more thiadiazole segments, the resonance of the acceptor moiety becomes stronger, which further stabilizes the delocalized electrons. It can be seen that **DMBI-BDZC** has a high-lying HOMO (−3.84 eV), comparable to all **rNDI**-based polymers, and doping by the conventional ground-state integer charge transfer (ICT) process requires the donation of electrons from the HOMO of the dopant to the LUMO of the host polymer semiconductor. For these reasons, these energetics suggest that ground-state ICT between the dopant and the **rNDI**-based polymer is indeed a plausible mechanism that could lead to n-type doping. The difference in resonance would make the mobility significantly different with doping, which will be discussed later.

https://doi.org/10.1021/acsami.2c23067
ACS Appl. Mater. Interfaces 2023, 15, 15745−15757

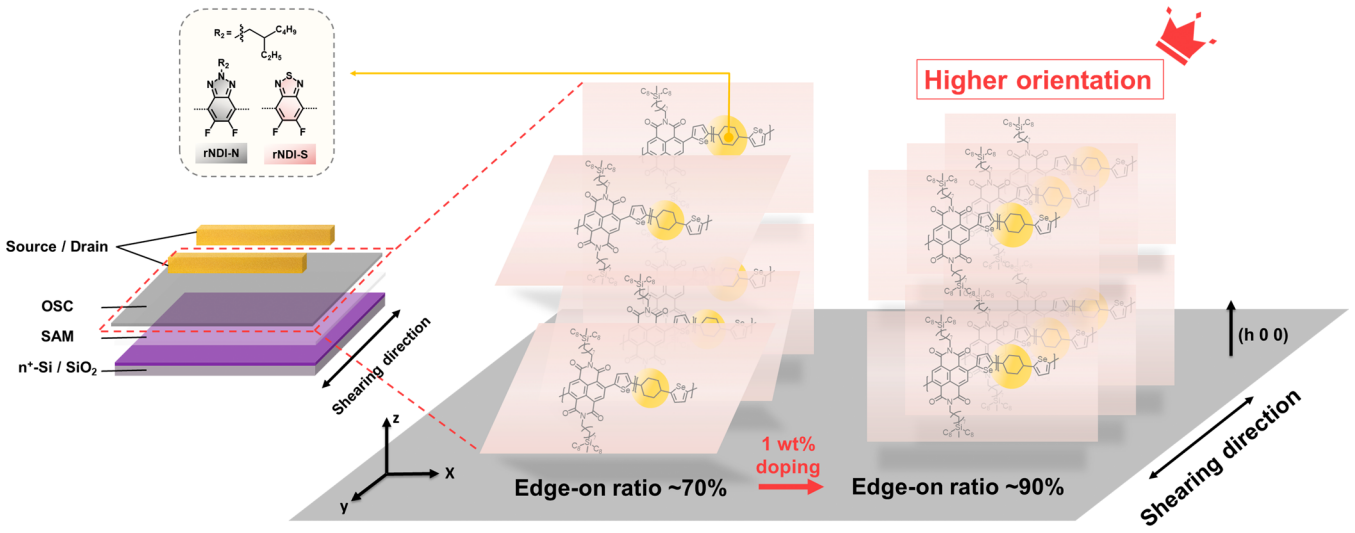

Figure 4. Representation of 1 wt % doping consequence in crystalline orientation for **rNDI-N/S**.

Electron Paramagnetic Resonance (EPR) Measurements. To further evaluate the doping effect of **DMBI-BDZC** on these four **rNDI**-based polymers, solution EPR measurements were performed at a fixed doping level of 1 wt % **DMBI-BDZC**. The EPR measurement allows direct detection of unpaired or free electrons and is widely used in organic semiconductors to determine doping efficiency.[51,52] As shown in Figure 2a,b, weak EPR signals were observed for the undoped **rNDI-N/S**, indicating its good diamagnetic properties. However, after the addition of dopant to the **rNDI-N/S** solution, strong signals of paramagnetic radical species were observed. These results suggest that the charge transfer between **rNDI-N/S** and dopant induces an effective n-doping of the polymer semiconductor.[53,54] In contrast, for the undoped **rNDI-NN** and **rNDI-SS** (Figure 2c,d), both samples produced clearly noticeable EPR signals. This is an indication of pro-quinoidal structures of **rNDI-NN/-SS** copolymers, characteristic of the open-shell resonance (Figure S14).[55,56] The small shoulder peak at the magnetic field of ~3505 G observed in **rNDI-SS** should be attributed to the impurities and defects.[57] We also observe that the EPR signal remains similar for doped **NDI-NN/rNDI-SS** solutions. This is due to the higher comformation of coplanarity with their extended pro-quinoidal characters along the polymer backbone,[36,58] which possess difficulties for further doping.

Thin-Film Morphology and Microstructure. We next used atomic force microscopy (AFM) and grazing incidence wide-angle X-ray scattering (GIWAXS) analysis to characterize the film morphology and microstructure of undoped and doped **rNDI**-based random D−A copolymers and to compare the molecular packing of copolymers with different acceptor units. Figures S15−S18 show the morphologies of undoped and doped films by AFM, including phase and height profiles. All of these four undoped **rNDI**-based polymer films exhibited relatively smooth surfaces, consistently presenting a subnanometric root-mean-square roughness (R_{rms}: 0.6−1.4 nm), with small granular aggregates (tens of nanometers in size) randomly distributed on the surface. A slightly higher R_{rms} of **rNDI-NN/SS** than **rNDI-N/S** is probably contributed by the increased coplanarity of the pro-quinoidal structures.[55] In addition, the introduction of a small amount of dopant does not cause any change in the film morphology and R_{rms}, providing evidence of good miscibility between the dopant and the polymer matrix.

The film microstructures and molecular packing of polymer chains were investigated using 2D GIWAXS (Figure 3). In Figure 3a, the undoped **rNDI-N/S** films show lamellar stacking reflections (h00) primarily in the out-of-plane direction (q_z), indicating a predominantly edge-on orientation. For the undoped **rNDI-NN/SS** films, the diffraction of face-on stacking appears in the q_{xy} direction and coexists with the edge-on stacking. The bimodal molecular arrangement implies less oriented crystallites, resulting in less efficient charge transport properties. The out-of-plane linecuts of the GIWAXS spectra for the four undoped polymer films are plotted in Figure 3c. Their lamellar stacking (100) distances are determined to be 3.07, 2.89, 3.05, and 3.14 nm for **rNDI-N/S/NN/SS**, respectively. The GIWAXS linecuts also reveal that both **rNDI-N** and **rNDI-NN** polymers have substantial long-range order with scattering reflexes up to the third order in the (h00) stacking direction, indicating the highly ordered lamellar packing of the polymer side chains. None of the four samples exhibit strong $\pi-\pi$ stacking features in both out-of-plane and in-plane directions.

The microstructural changes of the doped polymer films were further evaluated. Figure 3b−f also exhibits well-defined (h00) diffraction patterns along the q_z direction for **rNDI-N/S** films with doping concentrations of 1−4 wt %. The polymer backbone orientation is controlled by solution doping process, which endows the packing property. As shown in Figure 3f, both **rNDI-N/S** films at 1 wt % doping show a decreased lamellar stacking distance compared to the undoped films, and this spacing gradually increases with further increase in dopant. At a low doping level (1 wt %), (100) diffraction peaks are narrower and sharper, and the coherence lengths estimated from the Scherrer equation increase from 12 to 20 nm for **rNDI-N** and from 19 to 21 nm for **rNDI-S** before and after 1 wt % doping, respectively, accompanied by a decreased lamellar stacking, this suggests an increase in crystallite size and crystalline order.[59] Furthermore, estimated from the intensity vs Azimuthal angle profiles in Figure 3d,e, the fractions of the edge-on orientation are 95 and 91% for **rNDI-N/S** at 1 wt % doped, respectively, significantly increasing from ~70% of the undoped ones, which reveals a higher orientation

https://doi.org/10.1021/acsami.2c23067
ACS Appl. Mater. Interfaces 2023, 15, 15745−15757

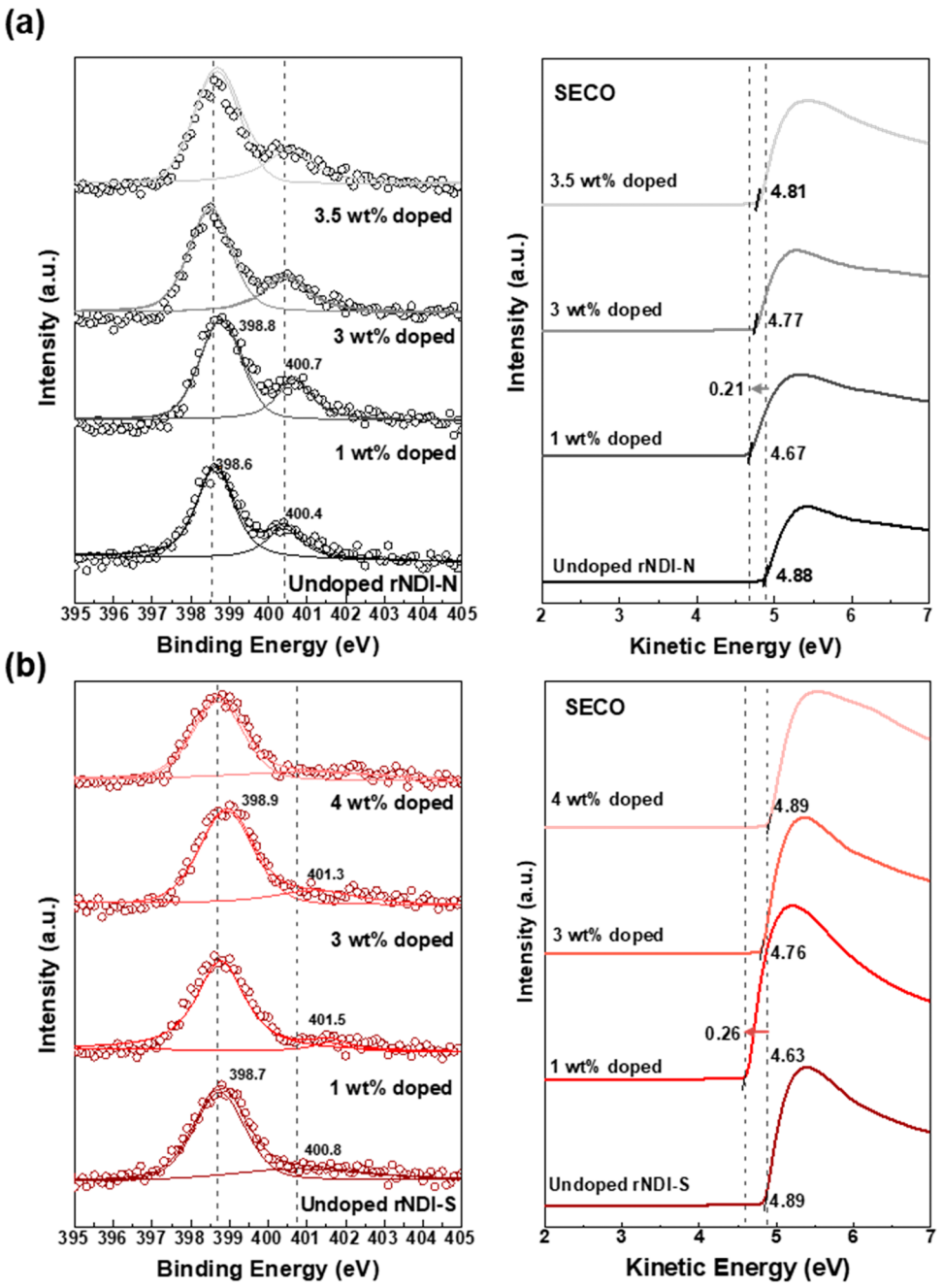

Figure 5. XPS spectra of N 1s signal and UPS secondary electron cutoff (SECO) of the (a) **rNDI-N** and (b) **rNDI-S** films with dopant concentrations varying from 0 to 4 wt %.

caused by the dopant (Figure 4). The molecular packing in **rNDI-N/S** films with 1 wt % doping, the crystalline orientation enhancement, where the charge transport was thought to prefer the higher fractions of edge-on orientation for the charge hopping between polymer chains, might lead to superior OFET performance. At higher doping levels, the intercalation of more dopants into the side chains expands the lamellar stacking distance (Figure 3f), which adversely affects the OFET performance.[59] However, no particular difference between the doped **rNDI-NN/SS** samples was found from the 2D GIWAXS patterns and 1D profiles (Figure 3f), which is in agreement with the EPR measurements. (Figure 2c,d).[55] The addition of the dopant to the **rNDI-NN/SS** polymers does not significantly hinder the molecular packing of the polymer chains.

X-ray Photoelectron Spectra (XPS) and Ultraviolet Photoelectron Spectra (UPS) Studies. To further characterize the doping states, X-ray photoelectron spectra (XPS) and ultraviolet photoelectron spectra (UPS) of the **rNDI-NN/SS** copolymers and their doped films were measured, as shown in Figure 5. The high-resolution XPS spectra of N 1s of undoped polymer film were fitted by two peaks (Figure 5a,b). The peaks centered at ~398.5 and 400 eV are in accordance with the cyanide and amide groups of **rNDI-N/S**, respectively.[60,61] However, these two peaks shifted at higher binding energy appear in all of the doped polymer films due to the greater electronegativity of **DMBI-BDZC**, which is

https://doi.org/10.1021/acsami.2c23067
ACS Appl. Mater. Interfaces 2023, 15, 15745−15757

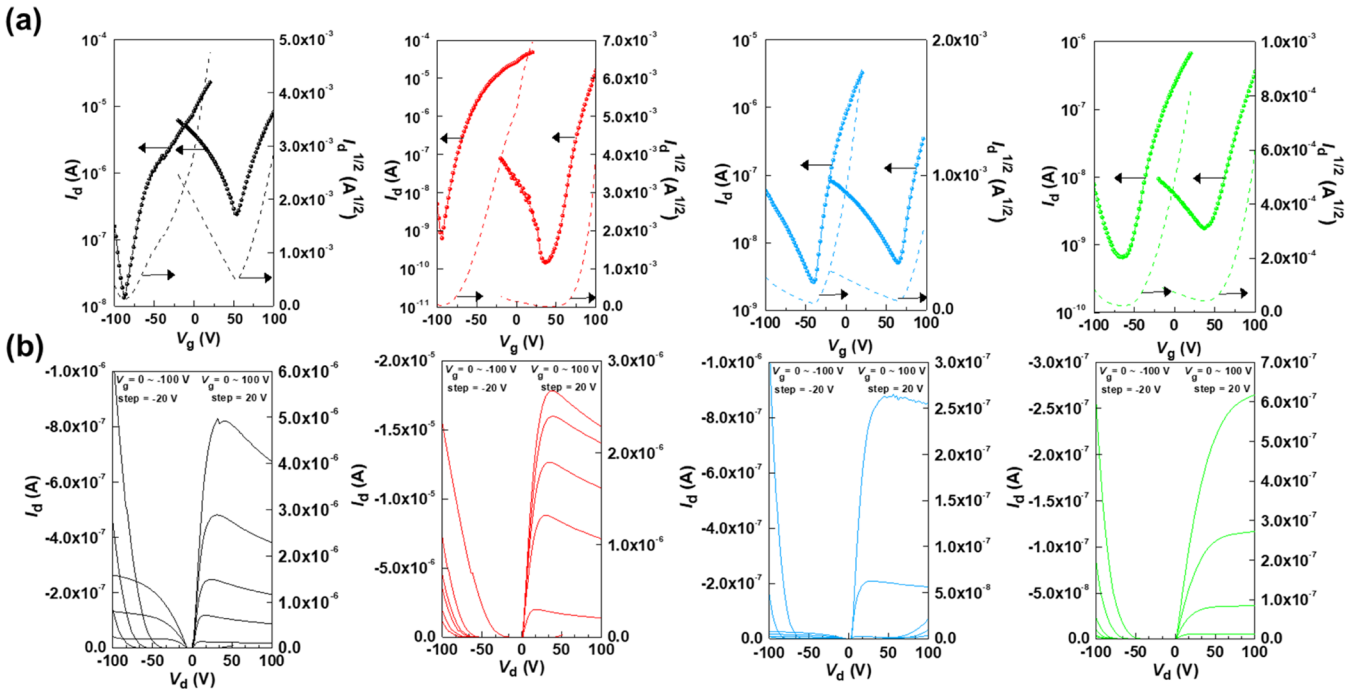

Figure 6. (a) Transfer and (b) output curves of the OFET devices in four undoped **rNDI**-based polymer films.

Table 2. OFET Performance of Undoped and Doped rNDI-Based Polymers

	n-channel			p-channel		
	μ_{max} ($cm^2\ V^{-1}\ s^{-1}$)	I_{ON}/I_{OFF} (-)	V_{th} (V)	μ_{max} ($cm^2\ V^{-1}\ s^{-1}$)	I_{ON}/I_{OFF} (-)	V_{th} (V)
undoped **rNDI-N**	1.43×10^{-2}	10^3 to 10^4	71.8 ± 1.3	2.40×10^{-3}	10^3 to 10^4	−85.0 ± 3.5
1 wt % doped **rNDI-N**	8.00×10^{-2}	10^3 to 10^4	71.4 ± 1.3	2.99×10^{-3}	10^3 to 10^4	−84.8 ± 1.5
3 wt % doped **rNDI-N**	3.45×10^{-2}	10^3 to 10^4	69.4 ± 1.8	2.23×10^{-3}	10^3 to 10^4	−82.0 ± 2.2
3.5 wt % doped **rNDI-N**	1.42×10^{-2}	10^1 to 10^2	57.8 ± 1.6	7.30×10^{-3}	10^2 to 10^3	−79.4 ± 5.3
undoped **rNDI-S**	5.39×10^{-2}	10^5 to 10^6	79.9 ± 0.5			
1 wt % doped **rNDI-S**	1.75×10^{-1}	10^5 to 10^6	78.3 ± 0.3			
3 wt % doped **rNDI-S**	6.88×10^{-2}	10^4 to 10^5	76.0 ± 0.8			
4 wt % doped **rNDI-S**	1.50×10^{-1}	10^4 to 10^5	73.5 ± 0.3			
undoped **rNDI-NN**	8.79×10^{-3}	10^2 to 10^3	81.5 ± 8.3	8.21×10^{-5}	10^2 to 10^3	−62.2 ± 15.7
0.5 wt % doped **rNDI-NN**	3.13×10^{-3}	10^2 to 10^3	76.4 ± 3.3	7.61×10^{-5}	10^2 to 10^3	−50.9 ± 6.8
1 wt % doped **rNDI-NN**	3.20×10^{-3}	10^2 to 10^3	75.5 ± 0.7	2.98×10^{-6}	10^2 to 10^3	−43.4 ± 5.0
undoped **rNDI-SS**	1.01×10^{-3}	10^2 to 10^3	69.6 ± 10.3	4.31×10^{-5}	10^1 to 10^2	−71.8 ± 20.3
1 wt % doped **rNDI-SS**	2.41×10^{-4}	10^2 to 10^3	49.8 ± 0.9	1.49×10^{-5}	10^2 to 10^3	−29.8 ± 3.6

considered as an interaction between the host polymer and the dopant.[61,62] It also should be noted that the peak intensities in doped films do not vary with increasing dopant due to the low doping ratio. Although the shift in energetic positions is not that large, the XPS results still demonstrate an effective doping process in the **rNDI-N/S** copolymers. The doping procedure and precise energy levels were also supported by the UPS measurement for undoped **rNDI-N/S** films and doped films with various doping concentrations (Figure 5a,b). From undoped to doped polymer films, the upshifted Fermi level toward the LUMO energy level of polymers clearly demonstrates the increase in electron density due to successful n-doping. Through the free charge carriers generated by the doping process, it is evident that the 1 wt % n-doping exhibits the largest upward shift, which may be due to the more ordered crystalline domains of both polymer films.[63,64] This result is consistent well with the microstructural crystallinity of doped **rNDI-N/S** films from the GIWAXS measurement (Figure 3). The samples doped by higher doping levels (3−4 wt %) show the downshifted Fermi levels than those by 1 wt %, which may be correlated with their higher trap densities (will be discussed below).

OFET Characterization. To investigate the correlation between the acceptor moieties and their thin-film microstrurctures in **rNDI**-based polymers and charge transport properties, four donor−acceptor conjugated polymers were tested in OFETs with bottom-gate top-contact (BGTC) architectures. The organic semiconductors were solution-sheared on the ODTS-treated Si/SiO_2 substrate using Au as top-contact electrodes, as detailed in the Experimental Section. Figure 6 shows the transfer and output characteristics of these **rNDI**-based polymers-based OFETs studied under nitrogen-filled conditions, and Table 2 summarizes the calculated n- and p-channel properties, including the electron (μ_e) and hole mobility (μ_h), the ON/OFF ratio (I_{ON}/I_{OFF}), and the threshold voltage (V_{th}). The average mobilities (μ_{avg}) with error bars for each polymer were measured from at least 10 different devices. All **rNDI-N/NN/SS** polymers show

https://doi.org/10.1021/acsami.2c23067
ACS Appl. Mater. Interfaces 2023, 15, 15745−15757

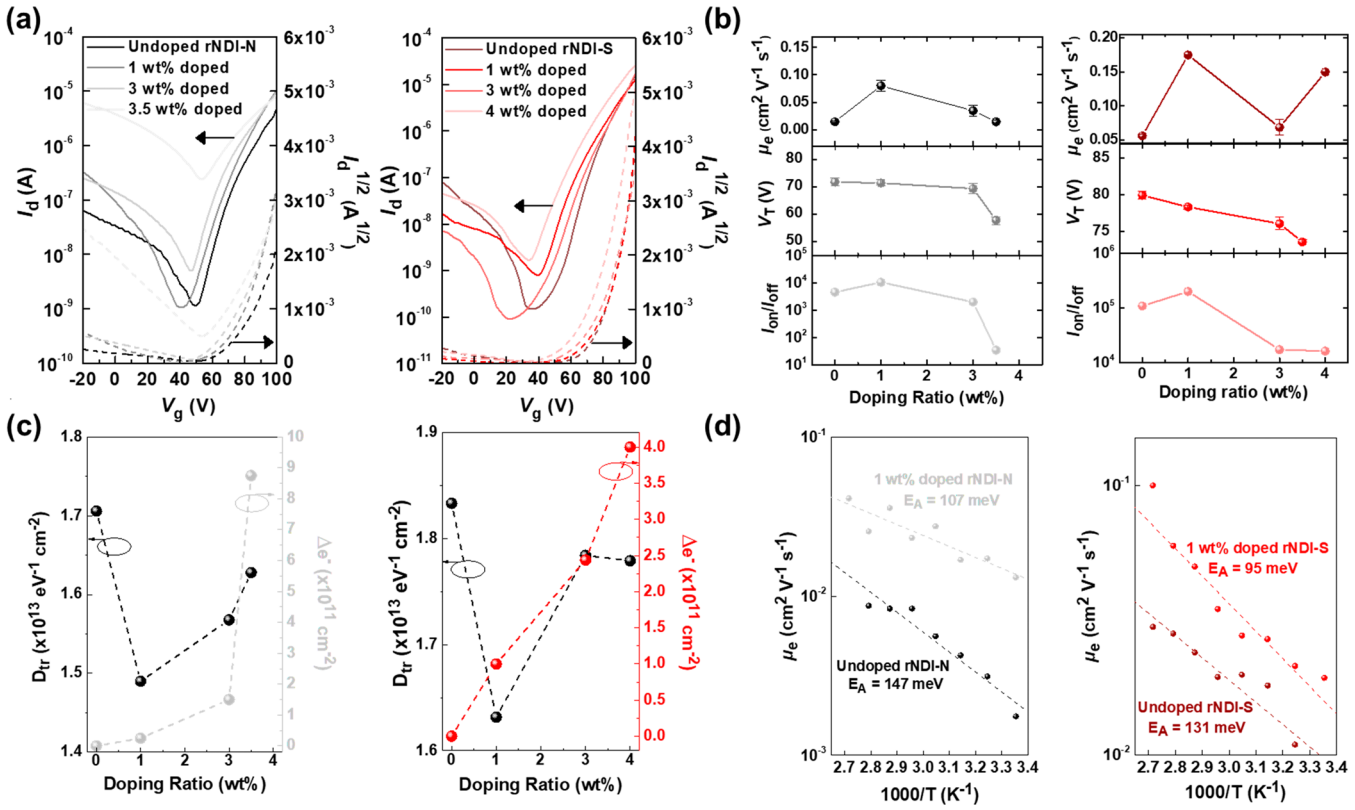

Figure 7. (a) Transfer curves of the OFET devices, (b) electron mobility (μ_e) in saturation regime, threshold voltage (V_{th}) variation as a function of the doping ratio (wt %) and ON/OFF ratio (I_{ON}/I_{OFF}), (c) excess of induced electrons (Δe^-) and interfacial trap density (D_{tr}) of undoped **rNDI-N/S** with dopant concentrations varying from 0 to 4 wt %, and (d) temperature dependence of μ_e and calculated activation energy (E_A) for undoped and 1 wt % doped **rNDI-N/S**.

ambipolar transport behavior,[65] except for **rNDI-S** showing unipolar n-channel OFET performance, although μ_e is higher than μ_h. The maximum μ_e and μ_h for ambipolar **rNDI-NN/SS** are similar in the order of $\sim 10^{-3}$ and $\sim 10^{-5}$ cm^2 V^{-1} s^{-1}, respectively. Comparatively, **rNDI-N** OFET exhibits 1−2 orders of magnitude greater μ_e and μ_h than **rNDI-NN/SS**. The device based on **rNDI-N** gives a maximum μ_e of 1.43 × 10^{-2} cm^2 V^{-1} s^{-1}. The relatively low mobility of **rNDI-NN/SS** is attributed to the fewer oriented crystallites with the coexisting edge-on/face-on bimodel orientation and lower ordering of lamellar packing, as discussed earlier (Figure 3), which limits the efficient charge transport. In addition, the low-lying LUMO energy levels of **rNDI-S** favor electron injection, but the deep HOMO energy level (−5.72 eV) greatly inhibits hole accumulation, resulting in a unipolar n-type channel with a maximum μ_e of 5.39 × 10^{-2} cm^2 V^{-1} s^{-1}.[65] The I_{ON}/I_{OFF} ratios of the devices obtained from **rNDI-NN/SS** are in the range of 10^1 to 10^3 for both p- and n-channel operations. However, **rNDI-N/S** devices present a relatively large I_{ON}/I_{OFF} ratio of 10^3 to 10^5. The small I_{ON}/I_{OFF} ratio of the pro-quinoidal structures of **rNDI-NN/SS** suggests the presence of excess charge carriers, which is consistent with their biradical characters observed in EPR measurement (Figure 2).[66]

To evaluate the effect of dopants on the charge transport properties of **rNDI**-based polymers, different dopant concentrations within these four polymer films are applied for OFET performance optimization.[55] Figures 7a,b and S21 show the resulting transfer cures of doped **rNDI-N/S** and **rNDI-NN/SS**, respectively, and the corresponding (drain current)$^{1/2}$ vs gate voltage from which both V_{th} and μ_e (or μ_h) can be determined. Key device performance data based on doped **rNDI**-based copolymers as a function of doping concentration are provided in Table 2. The analysis of these data leads to the following results. In the case of doped **rNDI-NN/SS** devices, they show similar or even decreased μ_e and μ_h values, which is attributed to the proquinodal structures and the invariant molecular orientation of both polymers, as evidenced by the EPR (Figure 2) and GIWAXS (Figure 3) results, respectively. Apparently, dopants were found to have a profound effect on **rNDI-N/S**-based OFETs with a clear indication of n-doping. Figure 7b shows the variation of μ_e, I_{on}/I_{off}, and V_{th} for doping concentrations from 0 to 4 wt %. The maximum μ_e is achieved by doping **rNDI-N/S** with 1 wt % dopant, leading to more than 6- and 3-fold enhancement compared to the undoped ones. This is explained by the enhanced crystallinity exerted by the 1 wt % doping, which is confirmed in the GIWAXS results (Figure 3). In addition, the maximum upshifted Fermi level toward LUMO energy level may generate free charge carriers for the semiconducting channels. Further increase in doping concentration (3−4 wt %) leads to a gradual decrease in μ_e. Also, it can be seen that the I_{on}/I_{off} and V_{th} of the doped **rNDI-N/S** OFETs decrease at high doping levels. The decrease in I_{on}/I_{off} is mainly due to the large increase in I_{off} (more than 10^{-8} A), which is the expected result since doping enhances the intrinsic conductivity. The shift to smaller V_{th} is explainable because the trap state is filled by doping-induced carriers. Thus, the addition of dopants within the conjugated polymer films affects the electrical properties. The μ_e stability of 1 wt % doped **rNDI-N** sample was also measured. Device performance of doped **rNDI-N** OFET stored at a relative humidity of ∼40%

https://doi.org/10.1021/acsami.2c23067
ACS Appl. Mater. Interfaces 2023, 15, 15745−15757

and room temperature was monitored periodically for 10 weeks. Figure S22 shows that the doped **rNDI-N** device exhibits high ambient stability while still maintaining 70% of the initial μ_e after 2 months.

It is known that effective doping at the appropriate level also introduces charges contributed by the dopant, which contributes to enhanced charge transport. Here, the number of charges caused by doping is estimated from the transistor characteristics, as shown in eq 2[67−70]

$$\Delta e^- = C_i e^{-1} |V_{th(doped)} - V_{th(undoped)}| \quad (2)$$

where C_i is the capacitance per unit area of the SiO_2 dielectric layer, e is the elementary charge, and V_{th} is the threshold voltage. The negative shifts of V_{th} in the n-doped **rNDI-N/S** films can be considered as the number of induced electrons (Δe^-) at the semiconductor/dielectric interface after doping.[46] As shown in Figure 7c, Δe^- increases simultaneously with increasing dopant concentration for both doped films, reaching the highest [$(4-9) \times 10^{11}$ cm^{-2}] at 3.5 and 4 wt % doping levels, respectively. The doping-induced electrons were also interpreted as a slight increase in the observed OFF current (Figure 7c), so the dopant successfully served as an n-type dopant for both polymer films. It has also been reported that the enhanced mobility due to molecular doping is due to the screening effect on the preexisting traps within the films by the excess charges generated, which is mainly associated with the passivation of trap states and the reduction of the contact resistance (R_c).[67] To investigate how the generation of excess charges impacts the concentration of trap states and influences the performance of resulting OFETs, the trap density (D_{tr}) was calculated using eq 3.[67,68,70]

$$D_{tr} = \frac{C_i}{e}\left(\frac{eSS}{k_B T \ln(10)} - 1\right) \quad (3)$$

where C_i is the capacitance per unit area of the SiO_2 dielectric layer, e is the elementary charge, SS is the subthreshold swing, k_B is the Boltzmann constant, and T is the absolute temperature. The D_{tr} of both doped **rNDI-N/S** films was found to decrease at 1 wt % doping (Figure 7c) and subsequently increase at higher doping levels. It is clear that 1 wt % doping presents the lowest D_{tr} and the evolution of D_{tr} is consistent with the variation of μ_e, which is mainly attributed to the improvement of the microstructure crystallinity analyzed by GIWAXS (Figure 3). The R_c analysis using the transmission line method (TLM; calculated by the data in Figure S23) is further investigated. The channel-width-normalized contact resistance (R_cW) is determined for a set of OFETs with channel lengths (L) from 30 to 80 μm. Figure S24 shows the R_cW vs V_g for undoped and doped **rNDI-N/S** devices. It can be seen that the R_cW of the doped devices is significantly smaller than that of the undoped ones, which is explained by the more edge-on orientation of the doped samples (Figures 3 and 4). Finally, the variation of the properties of undoped and doped **rNDI-N/S** OFETs in the range of 298−371 K as a function of the temperature inverse was recorded. We observe that μ_e decreases with decreasing temperature for all systems, which is consistent with thermally activated transport in organic semiconductors (Figure 7d). By fitting the temperature-dependent μ_e with the Arrhenius model, the activation energy (E_A) of the undoped and doped samples can be quantified. As shown in Figure 7d, n-doping of **rNDI-N/S** reduces the E_A from 147 meV (**rNDI-N**) and 131 meV (**rNDI-S**) to 107 meV (1 wt % doped **rNDI-N**) and 95 meV (1 wt % doped **rNDI-S**), a reduction of ∼40 meV. The reduction in E_A of the doped samples implies that additional charge carriers effectively fill the trap and the associated shift of E_F to LUMO.[62]

Correlations between Morphology and Energy Levels/OFET Characterization. Overall, a schematic mechanism of **DMBI-BDZC** doping to improve the charge transport properties of copolymers is proposed in Figure S25. To induce electron transfer, the HOMO energy level of the n-type **DMBI-BDZC** dopant is close to the LUMO of the **rNDI-N/S** copolymers. Thus, the dopant can donate electrons from HOMO to the unfilled band of the polymer, which interacts with the traps of **rNDI-N/S**. This n-type doping of the host polymer can be demonstrated by the upward shift of E_F toward the LUMO energy level from the undoped films to the doped films (Figures 5 and S25), indicating an increase in electron density. It also shows an increase in the induced Δe^- measured from the V_{th} shift. In addition, the decrease in D_{tr}, R_C, and E_A and the improvement in microstructural crystallinity suggest that the n-doping process helps to resolve the disorder/trap region of the undoped semicrystalline **rNDI-N/S**, which enhances the μ_e of the doped OFETs. The improved crystallinity (by microstructural and spectroscopic analysis) and the associated reduction of energetic disorder (from lower E_A) lead to suppression of trap state (from lower D_{tr}) in the doped conjugated polymer films.

CONCLUSIONS

In conclusion, we synthesized branched methyl(8-bromooctyl)-dioctylsilyl-containing **NDI** monomer with electron-donating selenophene linkers, which were copolymerized with four acceptors (**N**, **S**, **NN**, and **SS**) to obtain a series of soluble **rNDI**-based random copolymers (**rNDI-N/S/NN/SS**). The incorporation of acceptors with different electron-withdrawing strengths in the copolymers allows manipulation of the HOMO/LUMO energy levels, film morphologies, molecular microstructures, and charge transport properties in OFETs. **rNDI-N/NN/SS** copolymers show the ambipolar behavior, whereas **rNDI-S** shows unipolar n-channel characteristics because the relatively deep HOMO energy greatly suppresses hole accumulation. Although **rNDI-NN/SS** copolymers containing pro-quinoidal moieties lead to red-shifted absorption and polaron delocalization, the limited OFET mobility is mainly due to their mixed edge-on/face-on bimodal molecular orientation, resulting in less ordering of undoped samples. By introducing an n-type **DMBI-BDZC** dopant into the **rNDI-N/S** copolymers, enhanced μ_e in OFETs is observed through improved crystallinity, more edge-on ordering, trap filling, and lower R_C/E_A coexistence, resulting in more efficient electron transport. However, the μ_e of the doped **rNDI-NN/SS** copolymers does not change or even decrease. By optimizing the doping level at 1 wt %, the μ_e of doped **rNDI-N/S** copolymers are all $\sim 10^{-1}$ cm^2 V^{-1} s^{-1}, which is 3- to 6-fold enhancement compared to undoped OFETs. The good environmental stability of the doped **rNDI-N** sample was also highlighted, with largely maintained μ_e after 2 months of exposure to ambient atmosphere. This work describes the molecular design of acceptor moieties in **NDI**-based random copolymers and the doping strategy to improve the charge transport ability.

https://doi.org/10.1021/acsami.2c23067
ACS Appl. Mater. Interfaces 2023, 15, 15745−15757

■ ASSOCIATED CONTENT

Supporting Information

The Supporting Information is available free of charge at https://pubs.acs.org/doi/10.1021/acsami.2c23067.

Synthesis details; instrumentation; ^{1}H NMR spectrum; TGA/DSC thermograms; cyclic voltammetry (CV) plots; high spin pro-quinoidal structures; AFM images; GIWAXS patterns; transfer and output curves of the OFETs; contact resistance (R_cW) vs V_g plots; and doping mechanism scheme (PDF)

■ AUTHOR INFORMATION

Corresponding Authors

Chu-Chen Chueh − *Department of Chemical Engineering and Advanced Research Center for Green Materials Science and Technology, National Taiwan University, Taipei 10617, Taiwan;* orcid.org/0000-0003-1203-4227; Email: cchueh@ntu.edu.tw

Cheng-Liang Liu − *Department of Materials Science and Engineering and Advanced Research Center for Green Materials Science and Technology, National Taiwan University, Taipei 10617, Taiwan;* orcid.org/0000-0002-8778-5386; Email: liucl@ntu.edu.tw

Authors

Yun Chang − *Department of Materials Science and Engineering, National Taiwan University, Taipei 10617, Taiwan*

Ying-Sheng Wu − *Department of Chemical Engineering, National Taiwan University, Taipei 10617, Taiwan*

Shih-Huang Tung − *Institute of Polymer Science and Engineering, National Taiwan University, Taipei 10617, Taiwan;* orcid.org/0000-0002-6787-4955

Wen-Chang Chen − *Department of Chemical Engineering and Advanced Research Center for Green Materials Science and Technology, National Taiwan University, Taipei 10617, Taiwan;* orcid.org/0000-0003-3170-7220

Complete contact information is available at: https://pubs.acs.org/10.1021/acsami.2c23067

Author Contributions

$^{\perp}$Y.C. and Y.-S.W. contributed equally to this work.

Notes

The authors declare no competing financial interest.

■ ACKNOWLEDGMENTS

The authors gratefully thank the financial support from the Ministry of Education (111L9006) and the National Science and Technology Council (NSTC) in Taiwan (111-2634-F-002-016). C.-C.C. also thanks the financial support from the NSTC in Taiwan (111-3116-F-011-006, 111-2628-E-002-009, 109-2628-E-002-008-MY3, and 111-2124-M-002-021) and from Top University Project of National Taiwan University (NTU) (111L7818). C.-L.L. gratefully acknowledges the financial support from 2030 Cross-Generation Young Scholars Program by NSTC in Taiwan, under Grant 111-2628-E-002-014. The authors thank Beamline B17A1 from the National Synchrotron Radiation Research Center (NSRRC) of Taiwan for providing beamtime. The authors thank Shou-Ling Huang for the assistance in NMR experiments at the Instrumentation Center at NTU.

■ REFERENCES

(1) Lin, W. P.; Liu, S. J.; Gong, T.; Zhao, Q.; Huang, W. Polymer-Based Resistive Memory Materials and Devices. *Adv. Mater.* **2014**, *26*, 570−606.

(2) Chou, Y.-H.; Chang, H.-C.; Liu, C.-L.; Chen, W.-C. Polymeric Charge Storage Electrets for Non-Volatile Organic Field Effect Transistor Memory Devices. *Polym. Chem.* **2015**, *6*, 341−352.

(3) Mu, B.; Hsu, H.-H.; Kuo, C.-C.; Han, S.-T.; Zhou, Y. Organic Small Molecule-Based Rram for Data Storage and Neuromorphic Computing. *J. Mater. Chem. C* **2020**, *8*, 12714−12738.

(4) Wu, P.-H.; Lin, Y.-C.; Laysandra, L.; Lee, M.-H.; Chiu, Y.-C.; Isono, T.; Satoh, T.; Chen, W.-C. Organic−Inorganic Nanocomposite Film for High-Performance Stretchable Resistive Memory Device. *Macromol. Rapid Commun.* **2020**, *41*, No. 1900542.

(5) Koo, J. H.; Kim, D. C.; Shim, H. J.; Kim, T.-H.; Kim, D.-H. Flexible and Stretchable Smart Display: Materials, Fabrication, Device Design, and System Integration. *Adv. Funct. Mater.* **2018**, *28*, No. 1801834.

(6) Gao, H.; Chen, S.; Liang, J.; Pei, Q. Elastomeric Light Emitting Polymer Enhanced by Interpenetrating Networks. *ACS Appl. Mater. Interfaces* **2016**, *8*, 32504−32511.

(7) Root, S. E.; Savagatrup, S.; Printz, A. D.; Rodriquez, D.; Lipomi, D. J. Mechanical Properties of Organic Semiconductors for Stretchable, Highly Flexible, and Mechanically Robust Electronics. *Chem. Rev.* **2017**, *117*, 6467−6499.

(8) Hsieh, Y. T.; Chen, J. Y.; Fukuta, S.; Lin, P. C.; Higashihara, T.; Chueh, C. C.; Chen, W. C. Realization of Intrinsically Stretchable Organic Solar Cells Enabled by Charge-Extraction Layer and Photoactive Material Engineering. *ACS Appl. Mater. Interfaces* **2018**, *10*, 21712−21720.

(9) Li, Za.; Chueh, C.-C.; Jen, A. K. Y. Recent Advances in Molecular Design of Functional Conjugated Polymers for High-Performance Polymer Solar Cells. *Prog. Polym. Sci.* **2019**, *99*, No. 101175.

(10) Wang, S.; Xu, J.; Wang, W.; Wang, G. N.; Rastak, R.; Molina-Lopez, F.; Chung, J. W.; Niu, S.; Feig, V. R.; Lopez, J.; Lei, T.; Kwon, S. K.; Kim, Y.; Foudeh, A. M.; Ehrlich, A.; Gasperini, A.; Yun, Y.; Murmann, B.; Tok, J. B.; Bao, Z. Skin Electronics from Scalable Fabrication of an Intrinsically Stretchable Transistor Array. *Nature* **2018**, *555*, 83−88.

(11) Callaway, C. P.; Liu, A. L.; Venkatesh, R.; Zheng, Y.; Lee, M.; Meredith, J. C.; Grover, M.; Risko, C.; Reichmanis, E. The Solution Is the Solution: Data-Driven Elucidation of Solution-to-Device Feature Transfer for Π-Conjugated Polymer Semiconductors. *ACS Appl. Mater. Interfaces* **2022**, *14*, 3613−3620.

(12) Pan, Y.; Yu, G. Multicomponent Blend Systems Used in Organic Field-Effect Transistors: Charge Transport Properties, Large-Area Preparation, and Functional Devices. *Chem. Mater.* **2021**, *33*, 2229−2257.

(13) Wang, Y.; Sun, L.; Wang, C.; Yang, F.; Ren, X.; Zhang, X.; Dong, H.; Hu, W. Organic Crystalline Materials in Flexible Electronics. *Chem. Soc. Rev.* **2019**, *48*, 1492−1530.

(14) Chou, L.-H.; Na, Y.; Park, C.-H.; Park, M. S.; Osaka, I.; Kim, F. S.; Liu, C.-L. Semiconducting Small Molecule/Polymer Blends for Organic Transistors. *Polymer* **2020**, *191*, No. 122208.

(15) Kumagai, S.; Ishii, H.; Watanabe, G.; Yu, C. P.; Watanabe, S.; Takeya, J.; Okamoto, T. Nitrogen-Containing Perylene Diimides: Molecular Design, Robust Aggregated Structures, and Advances in N-Type Organic Semiconductors. *Acc. Chem. Res.* **2022**, *55*, 660−672.

(16) Zhang, C.; Zhu, X. N-Type Quinoidal Oligothiophene-Based Semiconductors for Thin-Film Transistors and Thermoelectrics. *Adv. Funct. Mater.* **2020**, *30*, No. 2000765.

(17) Wu, Y.; Zhao, Y.; Liu, Y. Toward Efficient Charge Transport of Polymer-Based Organic Field-Effect Transistors: Molecular Design, Processing, and Functional Utilization. *Acc. Mater. Res.* **2021**, *2*, 1047−1058.

(18) Kim, M.; Ryu, S. U.; Park, S. A.; Choi, K.; Kim, T.; Chung, D.; Park, T. Donor−Acceptor-Conjugated Polymer for High-Performance

Organic Field-Effect Transistors: A Progress Report. *Adv. Funct. Mater.* **2020**, *30*, No. 1904545.
(19) Huang, F.; Chen, K.-S.; Yip, H. L.; Hau, S. K.; Acton, O.; Zhang, Y.; Luo, J.; Jen, A. K.-Y. Development of New Conjugated Polymers with Donor−Π-Bridge−Acceptor Side Chains for High Performance Solar Cells. *J. Phys. Chem. B* **2009**, *131*, 13886−13887.
(20) Ajayaghosh, A. Donor-Acceptor Type Low Band Gap Polymers: Polysquaraines and Related Systems. *Chem. Soc. Rev.* **2003**, *32*, 181−191.
(21) Chen, J.; Yang, J.; Guo, Y.; Liu, Y. Acceptor Modulation Strategies for Improving the Electron Transport in High-Performance Organic Field-Effect Transistors. *Adv. Mater.* **2022**, *34*, No. 2104325.
(22) Zhang, Q.; Huang, J.; Wang, K.; Huang, W. Recent Structural Engineering of Polymer Semiconductors Incorporating Hydrogen Bonds. *Adv. Mater.* **2022**, *34*, No. 2110639.
(23) Lei, T.; Wang, J. Y.; Pei, J. Design, Synthesis, and Structure-Property Relationships of Isoindigo-Based Conjugated Polymers. *Acc. Chem. Res.* **2014**, *47*, 1117−1126.
(24) Al Kobaisi, M.; Bhosale, S. V.; Latham, K.; Raynor, A. M.; Bhosale, S. V. Functional Naphthalene Diimides: Synthesis, Properties, and Applications. *Chem. Rev.* **2016**, *116*, 11685−11796.
(25) Yuan, J.; Guo, W.; Xia, Y.; Ford, M. J.; Jin, F.; Liu, D.; Zhao, H.; Inganäs, O.; Bazan, G. C.; Ma, W. Comparing the Device Physics, Dynamics and Morphology of Polymer Solar Cells Employing Conventional Pcbm and Non-Fullerene Polymer Acceptor N2200. *Nano Energy* **2017**, *35*, 251−262.
(26) Guo, X.; Kim, F. S.; Seger, M. J.; Jenekhe, S. A.; Watson, M. D. Naphthalene Diimide-Based Polymer Semiconductors: Synthesis, Structure−Property Correlations, and N-Channel and Ambipolar Field-Effect Transistors. *Chem. Mater.* **2012**, *24*, 1434−1442.
(27) Park, K.; Shin, E. Y.; Jiao, X.; McNeill, C. R.; Kim, Y. H.; Kwon, S. K.; Noh, Y. Y. Effect of Backbone Sequence of a Naphthalene Diimide-Based Copolymer on Performance in N-Type Organic Thin-Film Transistors. *ACS Appl. Mater. Interfaces* **2019**, *11*, 35185−35192.
(28) Wei, H.; Liu, Y.; Liu, Z.; Guo, J.; Chen, P. A.; Qiu, X.; Dai, G.; Li, Y.; Yuan, J.; Liao, L.; Hu, Y. Effect of Backbone Fluorine and Chlorine Substitution on Charge-Transport Properties of Naphthalenediimide-Based Polymer Semiconductors. *Adv. Electron. Mater.* **2020**, *6*, No. 1901241.
(29) Yan, H.; Chen, Z.; Zheng, Y.; Newman, C.; Quinn, J. R.; Dötz, F.; Kastler, M.; Facchetti, A. A High-Mobility Electron-Transporting Polymer for Printed Transistors. *Nature* **2009**, *457*, 679−686.
(30) He, T.; Stolte, M.; Burschka, C.; Hansen, N. H.; Musiol, T.; Kälblein, D.; Pflaum, J.; Tao, X.; Brill, J.; Würthner, F. Single-Crystal Field-Effect Transistors of New Cl2-Ndi Polymorph Processed by Sublimation in Air. *Nat. Commun.* **2015**, *6*, No. 5954.
(31) Wang, Y.; Hasegawa, T.; Matsumoto, H.; Michinobu, T. Significant Improvement of Unipolar N-Type Transistor Performances by Manipulating the Coplanar Backbone Conformation of Electron-Deficient Polymers Via Hydrogen Bonding. *J. Am. Chem. Soc.* **2019**, *141*, 3566−3575.
(32) Zhao, Z.; Yin, Z.; Chen, H.; Zheng, L.; Zhu, C.; Zhang, L.; Tan, S.; Wang, H.; Guo, Y.; Tang, Q.; Liu, Y. High-Performance, Air-Stable Field-Effect Transistors Based on Heteroatom-Substituted Naphthalenediimide-Benzothiadiazole Copolymers Exhibiting Ultrahigh Electron Mobility up to 8.5 Cm V(-1) S(-1). *Adv. Mater.* **2017**, *29*, No. 1602410.
(33) Yuan, Z.; Buckley, C.; Thomas, S.; Zhang, G.; Bargigia, I.; Wang, G.; Fu, B.; Silva, C.; Brédas, J.-L.; Reichmanis, E. A Thiazole−Naphthalene Diimide Based N-Channel Donor−Acceptor Conjugated Polymer. *Macromolecules* **2018**, *51*, 7320−7328.
(34) Yum, S.; An, T. K.; Wang, X.; Lee, W.; Uddin, M. A.; Kim, Y. J.; Nguyen, T. L.; Xu, S.; Hwang, S.; Park, C. E.; Woo, H. Y. Benzotriazole-Containing Planar Conjugated Polymers with Noncovalent Conformational Locks for Thermally Stable and Efficient Polymer Field-Effect Transistors. *Chem. Mater.* **2014**, *26*, 2147−2154.
(35) Yuen, J. D.; Fan, J.; Seifter, J.; Lim, B.; Hufschmid, R.; Heeger, A. J.; Wudl, F. High Performance Weak Donor-Acceptor Polymers in Thin Film Transistors: Effect of the Acceptor on Electronic Properties, Ambipolar Conductivity, Mobility, and Thermal Stability. *J. Am. Chem. Soc.* **2011**, *133*, 20799−20807.
(36) Tam, T. L. D.; Ng, C. K.; Lim, S. L.; Yildirim, E.; Ko, J.; Leong, W. L.; Yang, S.-W.; Xu, J. Proquinoidal-Conjugated Polymer as an Effective Strategy for the Enhancement of Electrical Conductivity and Thermoelectric Properties. *Chem. Mater.* **2019**, *31*, 8543−8550.
(37) Liu, D.; Mun, J.; Chen, G.; Schuster, N. J.; Wang, W.; Zheng, Y.; Nikzad, S.; Lai, J. C.; Wu, Y.; Zhong, D.; Lin, Y.; Lei, Y.; Chen, Y.; Gam, S.; Chung, J. W.; Yun, Y.; Tok, J. B.; Bao, Z. A Design Strategy for Intrinsically Stretchable High-Performance Polymer Semiconductors: Incorporating Conjugated Rigid Fused-Rings with Bulky Side Groups. *J. Am. Chem. Soc.* **2021**, *143*, 11679−11689.
(38) Mun, J.; Ochiai, Y.; Wang, W.; Zheng, Y.; Zheng, Y. Q.; Wu, H. C.; Matsuhisa, N.; Higashihara, T.; Tok, J. B.; Yun, Y.; Bao, Z. A Design Strategy for High Mobility Stretchable Polymer Semiconductors. *Nat. Commun.* **2021**, *12*, No. 3572.
(39) Cassinelli, M.; Cimò, S.; Biskup, T.; Jiao, X.; Luzio, A.; McNeill, C. R.; Noh, Y.-Y.; Kim, Y.-H.; Bertarelli, C.; Caironi, M. Enhanced N-Type Doping of a Naphthalene Diimide Based Copolymer by Modification of the Donor Unit. *Adv. Electron. Mater.* **2021**, *7*, No. 2100407.
(40) Wang, S.; Sun, H.; Erdmann, T.; Wang, G.; Fazzi, D.; Lappan, U.; Puttisong, Y.; Chen, Z.; Berggren, M.; Crispin, X.; Kiriy, A.; et al. A Chemically Doped Naphthalenediimide-Bithiazole Polymer for N-Type Organic Thermoelectrics. *Adv. Mater.* **2018**, *30*, No. 1801898.
(41) Meng, B.; Liu, J.; Wang, L. Recent Development of N-Type Thermoelectric Materials Based on Conjugated Polymers. *Nano Mater. Sci.* **2021**, *3*, 113−123.
(42) Xu, Y.; Sun, H.; Liu, A.; Zhu, H.-H.; Li, W.; Lin, Y.-F.; Noh, Y.-Y. Doping: A Key Enabler for Organic Transistors. *Adv. Mater.* **2018**, *30*, No. 1801830.
(43) Lüssem, B.; Keum, C.-M.; Kasemann, D.; Naab, B.; Bao, Z.; Leo, K. Doped Organic Transistors. *Chem. Rev.* **2016**, *116*, 13714−13751.
(44) Scaccabarozzi, A. D.; Basu, A.; Aniés, F.; Liu, J.; Zapata-Arteaga, O.; Warren, R.; Firdaus, Y.; Nugraha, M. I.; Lin, Y.; Campoy-Quiles, M.; Koch, N.; Müller, C.; Tsetseris, L.; Heeney, M.; Anthopoulos, T. D. Doping Approaches for Organic Semiconductors. *Chem. Rev.* **2022**, *122*, 4420−4492.
(45) Han, J.; Ganley, C.; Hu, Q.; Zhao, X.; Clancy, P.; Russell, T. P.; Katz, H. E. Using Preformed Meisenheimer Complexes as Dopants for N-Type Organic Thermoelectrics with High Seebeck Coefficients and Power Factors. *Adv. Funct. Mater.* **2021**, *31*, No. 2010567.
(46) Panidi, J.; Kainth, J.; Paterson, A. F.; Wang, S.; Tsetseris, L.; Emwas, A. H.; McLachlan, M. A.; Heeney, M.; Anthopoulos, T. D. Introducing a Nonvolatile N-Type Dopant Drastically Improves Electron Transport in Polymer and Small-Molecule Organic Transistors. *Adv. Funct. Mater.* **2019**, *29*, No. 1902784.
(47) Lin, P.-S.; Shoji, Y.; Afraj, S. N.; Ueda, M.; Lin, C.-H.; Inagaki, S.; Endo, T.; Tung, S.-H.; Chen, M.-C.; Liu, C.-L.; Higashihara, T. Controlled Synthesis of Poly[(3-Alkylthio)Thiophene]S and Their Application to Organic Field-Effect Transistors. *ACS Appl. Mater. Interfaces* **2021**, *13*, 31898−31909.
(48) Wu, Y.-S.; Lin, Y.-C.; Hung, S.-Y.; Chen, C.-K.; Chiang, Y.-C.; Chueh, C.-C.; Chen, W.-C. Investigation of the Mobility−Stretchability Relationship of Ester-Substituted Polythiophene Derivatives. *Macromolecules* **2020**, *53*, 4968−4981.
(49) Ding, X.; Tran, D. K.; Kuzuhara, D.; Koganezawa, T.; Jenekhe, S. A. Comparative Study of Selenophene- and Thiophene-Containing N-Type Semiconducting Polymers for High Performance All-Polymer Solar Cells. *ACS Appl. Polym. Mater.* **2021**, *3*, 49−59.
(50) Kim, K.-H.; Park, S.; Yu, H.; Kang, H.; Song, I.; Oh, J. H.; Kim, B. J. Determining Optimal Crystallinity of Diketopyrrolopyrrole-Based Terpolymers for Highly Efficient Polymer Solar Cells and Transistors. *Chem. Mater.* **2014**, *26*, 6963−6970.
(51) Bredas, J. L.; Street, G. B. Polarons, Bipolarons, and Solitons in Conducting Polymers. *Acc. Chem. Res.* **1985**, *18*, 309−315.
(52) Han, Y.; Fei, Z.; Lin, Y.-H.; Martin, J.; Tuna, F.; Anthopoulos, T. D.; Heeney, M. Anion-Induced N-Doping of Naphthalenediimide

Polymer Semiconductor in Organic Thin-Film Transistors. *npj Flexible Electron.* **2018**, *2*, No. 11.
(53) Koh, C. W.; Heo, J. H.; Uddin, M. A.; Kwon, Y. W.; Choi, D. H.; Im, S. H.; Woo, H. Y. Enhanced Efficiency and Long-Term Stability of Perovskite Solar Cells by Synergistic Effect of Non-hygroscopic Doping in Conjugated Polymer-Based Hole-Transporting Layer. *ACS Appl. Mater. Interfaces* **2017**, *9*, 43846−43854.
(54) Pingel, P.; Arvind, M.; Kölln, L.; Steyrleuthner, R.; Kraffert, F.; Behrends, J.; Janietz, S.; Neher, D. P-Type Doping of Poly(3-Hexylthiophene) with the Strong Lewis Acid Tris-(Pentafluorophenyl)Borane. *Adv. Electron. Mater.* **2016**, *2*, No. 1600204.
(55) Chen, Z.; Li, W.; Sabuj, M. A.; Li, Y.; Zhu, W.; Zeng, M.; Sarap, C. S.; Huda, M. M.; Qiao, X.; Peng, X.; Ma, D.; Ma, Y.; Rai, N.; Huang, F. Evolution of the Electronic Structure in Open-Shell Donor-Acceptor Organic Semiconductors. *Nat. Commun.* **2021**, *12*, No. 5889.
(56) Ji, X.; Fang, L. Quinoidal Conjugated Polymers with Open-Shell Character. *Polym. Chem.* **2021**, *12*, 1347−1361.
(57) Seburg, R. A.; Patterson, E. V.; McMahon, R. J. Structure of Triplet Propynylidene (Hccch) as Probed by Ir, Uv/Vis, and Epr Spectroscopy of Isotopomers. *J. Am. Chem. Soc.* **2009**, *131*, 9442−9455.
(58) Kim, Y.; Kim, Y.-J.; Kim, Y.-A.; Jung, E.; Mok, Y.; Kim, K.; Hwang, H.; Park, J.-J.; Kim, M.-G.; Mathur, S.; Kim, D.-Y. Open-Shell and Closed-Shell Quinoid−Aromatic Conjugated Polymers: Unusual Spin Magnetic and High Charge Transport Properties. *ACS Appl. Mater. Interfaces* **2021**, *13*, 2887−2898.
(59) Li, H.; Xu, Z.; Song, J.; Chai, H.; Wu, L.; Chen, L. Single-Solution Doping Enabling Dominant Integer Charge Transfer for Synergistically Improved Carrier Concentration and Mobility in Donor−Acceptor Polymers. *Adv. Funct. Mater.* **2021**, *32*, No. 2110047.
(60) Nie, Q.; Wang, M.; Qiu, T.; Qiu, X. Density Functional Theory and Xps Studies of the Adsorption of Cyanide on Chalcopyrite Surfaces. *ACS Omega* **2020**, *5*, 22778−22785.
(61) Feng, K.; Guo, H.; Wang, J.; Shi, Y.; Wu, Z.; Su, M.; Zhang, X.; Son, J. H.; Woo, H. Y.; Guo, X. Cyano-Functionalized Bithiophene Imide-Based N-Type Polymer Semiconductors: Synthesis, Structure-Property Correlations, and Thermoelectric Performance. *J. Am. Chem. Soc.* **2021**, *143*, 1539−1552.
(62) Wang, Y.; Hasegawa, T.; Matsumoto, H.; Mori, T.; Michinobu, T. High-Performance N-Channel Organic Transistors Using High-Molecular-Weight Electron-Deficient Copolymers and Amine-Tailed Self-Assembled Monolayers. *Adv. Mater.* **2018**, *30*, No. 1707164.
(63) Liu, Y.; Villalva, D. R.; Sharma, A.; Haque, M. A.; Baran, D. Molecular Doping of a Naphthalene Diimide-Bithiophene Copolymer and Swcnts for N-Type Thermoelectric Composites. *ACS Appl. Mater. Interfaces* **2021**, *13*, 411−418.
(64) Bubnova, O.; Khan, Z. U.; Wang, H.; Braun, S.; Evans, D. R.; Fabretto, M.; Hojati-Talemi, P.; Dagnelund, D.; Arlin, J.-B.; Geerts, Y. H.; Desbief, S.; Breiby, D. W.; Andreasen, J. W.; Lazzaroni, R.; Chen, W. M.; Zozoulenko, I.; Fahlman, M.; Murphy, P. J.; Berggren, M.; Crispin, X. Semi-Metallic Polymers. *Nat. Mater.* **2014**, *13*, 190−194.
(65) Chen, J.; Yang, J.; Guo, Y.; Liu, Y. Acceptor Modulation Strategies for Improving the Electron Transport in High-Performance Organic Field-Effect Transistors. *Adv. Mater.* **2022**, *34*, No. e2104325.
(66) Dexter Tam, T. L.; Moudgil, A.; Teh, W. J.; Wong, Z. M.; Handoko, A. D.; Chien, S. W.; Yang, S.-W.; Yeo, B. S.; Leong, W. L.; Xu, J. Polaron Delocalization Dependence of the Conductivity and the Seebeck Coefficient in Doped Conjugated Polymers. *J. Phys. Chem. B* **2022**, *126*, 2073−2085.
(67) Ghamari, P.; Niazi, M. R.; Perepichka, D. F. Controlling Structural and Energetic Disorder in High-Mobility Polymer Semiconductors Via Doping with Nitroaromatics. *Chem. Mater.* **2021**, *33*, 2937−2947.
(68) Zhang, F.; Hu, Y.; Lou, Z.; Xin, X.; Zhang, M.; Hou, Y.; Teng, F. Interface Studies of Well-Controlled Polymer Bilayers and Field-Effect Transistors Prepared by a Mixed-Solvent Method. *RSC Adv.* **2018**, *8*, 11272−11279.
(69) Phan, H.; Wang, M.; Bazan, G. C.; Nguyen, T. Q. Electrical Instability Induced by Electron Trapping in Low-Bandgap Donor−Acceptor Polymer Field-Effect Transistors. *Adv. Mater.* **2015**, *27*, 7004−7009.
(70) Horowitz, G.; Delannoy, P. An Analytical Model for Organic-Based Thin-Film Transistors. *J. Appl. Phys.* **1991**, *70*, 469−475.

https://doi.org/10.1021/acsami.2c23067
ACS Appl. Mater. Interfaces 2023, 15, 15745−15757